The Astrophysical Journal, 732:117 (11pp), 2011 May 10 doi:10.1088/0004-637X/732/2/117

EVOLUTION OF CORONAL MASS EJECTION MORPHOLOGY WITH INCREASING HELIOCENTRIC DISTANCE. II. IN SITU OBSERVATIONS

N. P. Savani[1], M. J. Owens[2,3], A. P. Rouillard[4,5], R. J. Forsyth[3], K. Kusano[1,6], D. Shiota[7], R. Kataoka[8], L. Jian[9], and V. Bothmer[10]

[1] Solar-Terrestrial Environment Laboratory, Nagoya University, Nagoya, Japan; neel.savani02@imperial.ac.uk
[2] Space Environment Physic Group, University of Reading, Reading, UK
[3] The Blackett Laboratory, Imperial College London, London, UK
[4] College of Science, George Mason University, Fairfax, VA, USA
[5] Space Science Division, Naval Research Laboratory, Washington, DC, USA
[6] Japan Agency for Marine-Earth Science and Technology, Yokohama, Kanagawa 236-0001, Japan
[7] Computational Astrophysics Laboratory, Advanced Science Institute, RIKEN, Wako, Japan
[8] Interactive Research Center of Science, Tokyo Institute of Technology, Tokyo, Japan
[9] Institute of Geophysics and Planetary Physics, University of California, Los Angeles, CA, USA
[10] Institut für Astrophysik, Göttingen University, Göttingen, Germany
Received 2010 December 15; accepted 2011 March 8; published 2011 April 26

ABSTRACT

Interplanetary coronal mass ejections (ICMEs) are often observed to travel much faster than the ambient solar wind. If the relative speed between the two exceeds the fast magnetosonic velocity, then a shock wave will form. The Mach number and the shock standoff distance ahead of the ICME leading edge is measured to infer the vertical size of an ICME in a direction that is perpendicular to the solar wind flow. We analyze the shock standoff distance for 45 events varying between 0.5 AU and 5.5 AU in order to infer their physical dimensions. We find that the average ratio of the inferred vertical size to measured radial width, referred to as the aspect ratio, of an ICME is 2.8 ± 0.5. We also compare these results to the geometrical predictions from Paper I that forecast an aspect ratio between 3 and 6. The geometrical solution varies with heliocentric distance and appears to provide a theoretical maximum for the aspect ratio of ICMEs. The minimum aspect ratio appears to remain constant at 1 (i.e., a circular cross section) for all distances. These results suggest that possible distortions to the leading edge of ICMEs are frequent. But, these results may also indicate that the constants calculated in the empirical relationship correlating the different shock front need to be modified; or perhaps both distortions and a change in the empirical formulae are required.

Key words: Earth – shock waves – solar–terrestrial relations – Sun: coronal mass ejections (CMEs) – Sun: heliosphere

Online-only material: color figures

1. INTRODUCTION

In our companion paper (Savani et al. 2011, hereinafter referred to as Paper I), we discussed possible changes to the coronal mass ejection (CME) morphology as it propagates away from the Sun. This geometrical study investigated the radial propagation of a cylindrical flux rope and expressed quantitative values for the aspect ratio as it varied with heliocentric distance. As given in Paper I, the ratio between the out-of-ecliptic vertical size and radial width of a CME, defined as the aspect ratio, χ may be given by

$$\chi = \frac{R(r_0/L_0)}{r_0 + A(R - L_0)}, \quad (1)$$

where R is the heliocentric distance. The initial conditions of the cylindrical flux rope with a circular cross section are estimated to have a radius, $r_0 \sim 1$ solar radius (Rs), and start at a heliocentric distance, L_0 of $\sim 2Rs$. These initial conditions are reasonable estimates based on coronagraph observations. The rate of expansion, A, is defined as the quotient of the expansion velocity with the bulk flow of the CME (Owens 2006; Owens et al. 2006). Here the expansion velocity is defined as half the speed difference between the leading and trailing edges. Paper I showed that if A is defined to be a constant in a manner similar to a magnetic cloud model by Owens et al. (2006), then χ converges to a constant value defined by A and the total angular width, Ω. This would mean the morphology of the CME would become scale invariant and be contrary to the concept of a continually flattening CME structure, often referred to as "pancaking." However, if the constancy of A was relaxed to follow the estimates derived from statistical results from in situ measurements (Bothmer & Schwenn 1994; Liu et al. 2005; Wang et al. 2005), then the aspect ratio would no longer converge but flatten at an ever decreasing rate, such that the majority of the change would have already occurred by $\sim 150Rs$.

In this paper, we aim to estimate the non-radial extent of interplanetary CMEs (ICMEs). This is inferred by extrapolating our understanding of the physics of interplanetary bow shocks. Previously, attempts have been made to deduce a two-dimensional (2D) structure from measurements taken along a one-dimensional path that is generated as a CME passes over a spacecraft. Flux rope fittings to in situ data have played a powerful role in estimating the orientation and size of an ICME (e.g., Burlaga 1988; Lepping et al. 1990; Marubashi 1997; Mulligan & Russell 2001; Hu & Sonnerup 2002; Owens et al. 2006). While these techniques may attempt to deduce the size and orientation of the ICME, the shape is often an explicit assumption of the model used. MHD simulations (e.g., Riley et al. 2001; Manchester et al. 2004; Odstrcil et al. 2004; Lugaz et al. 2005; Kataoka et al. 2009; Nakamizo et al. 2009; Shiota et al. 2010) and interplanetary scintillation (IPS) studies (Jackson et al. 2007) have also significantly increased our understanding of

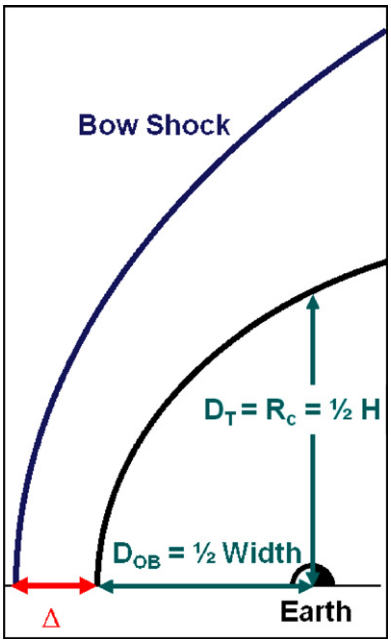

Figure 1. Schematic displaying the relationship between Earth's bow shock and characteristics of an ICME. We relate the width of a CME measured with in situ instruments and the distance from the Earth to the magnetopause nose, and the vertical size to the radius of curvature.

(A color version of this figure is available in the online journal.)

ICME morphology; but again do not provide direct observational evidence to the shape.

However, an attempt to deduce the 2D structure from direct measurements has been made by Russell & Mulligan (2002) and Liu et al. (2006); they estimated an aspect ratio of about 4 and 6, respectively. Russell & Mulligan investigated an event with a shock wave preceding a fast ICME. By measuring the sheath distance and shock orientation they were able to estimate a 2D cross section. Many of the assumptions from this analysis originate from a comparison between Earths bow shock and CME related interplanetary shocks (this is discussed further in Section 2).

Spreiter et al. (1966) produced a gas-dynamic model of the solar wind's interaction with a planetary body, and ignored all the magnetic forces on the flow. The magnetic field lines were assumed to convect with the fluid. The results of the model depend on the Mach number of the inflow, the polytropic index (γ), and the shape of the obstacle, which is of particular concern in this study.

When analyzing the shape and location of the bow shock, it is important to consider the standoff distance, Δ (see Figure 1). This is the perpendicular distance from the nose of the bow shock to the nearest obstacle edge (magnetopause). Spreiter et al. (1966) experimentally investigated metal models of the magnetosphere by firing them through argon gas at Mach numbers above 4.5. The authors showed a simple empirical formula could relate the shock standoff distance, Δ, to the distance between the center of Earth and the top of the obstacle boundary, $D_{\rm OB}$:

$$\frac{\Delta}{D_{OB}} = \frac{1.1\,\rho_\infty}{\rho_1}. \quad (2)$$

Here, ρ_∞ and ρ_1 are the mass density for upstream and downstream of the shock, respectively. The coefficient of 1.1 is produced by fitting a linear curve to the results. The authors expressed that this empirical relationship was robust for a wide range of conditions.

This work also produced the relationship of $D_T/D_{\rm OB} = 1.35$, where D_T is defined as the terminator distance. Later, Farris & Russell (1994) assumed that the value of this ratio defines the radius of curvature, R_c, of the obstacle—i.e., the curvature of the magnetopause boundary, or in our case, the ICME leading edge. The radius of curvature was then assumed to equal half the vertical size of the obstacle—i.e., half the vertical size of the ICME. Here, the vertical size refers to the length of the ICME that is perpendicular to both the heliocentric radial line and the axial direction of the assumed flux rope structure. This result is used later in Section 2 to infer the vertical size of an ICME, which is treated as a magnetic obstacle.

Siscoe & Odstrcil (2008) used physical arguments as well as an MHD simulation to investigate the properties of the sheath region between an ICME and its associated shock front. The authors proposed two different mechanisms for a sheath region with different characteristics: (1) "propagation sheath" is the traditional view of the solar wind entering the sheath region and moving around the object with a more-or-less steady-state flow, and then leaves the object behind; (2) "expansion sheath", which refers to a sheath region that forms around an expanding object that is not propagating relative to the solar wind. They believe ICME would behave as a hybrid of both these situations and argue that solar wind piles up in front of an ICME instead of flowing around it, resulting in an ICME sheath that is thinner than those of planetary magnetosheaths. This suggests our correlation of planetary sheaths and ICME sheaths may be misplaced, but their conclusions are yet to be supported observationally.

2. INTERPLANETARY CORONAL MASS EJECTION VERSUS BOW SHOCKS

Spreiter et al. (1966) measured the position of the bow shock empirically with the use of a wind tunnel and a model magnetosphere. This treatment allowed Russell & Mulligan (2002) to parameterize the radius of curvature of an ICME and correlate it to the shock standoff distance. The radius of curvature for an ICME leading edge is the result of both the bend in the magnetic rope axis and the curvature of the leading edge in the direction perpendicular to the plane containing the rope axis and the solar wind flow vector. Both of these dimensions are expected to be much larger than the radial thickness of the ICME measured in situ.

Landau & Lifshitz (1959) and Spreiter et al. (1966) related the shock Mach number to the density jump across the shock as follows:

$$\frac{\rho_\infty}{\rho_1} = \frac{(\gamma - 1)\,M_\infty^2 + 2}{(\gamma + 1)\,M_\infty^2}. \quad (3)$$

Here, M is the sound speed Mach number (namely, the ratio of the solar wind inflow speed to the upstream sound speed), ρ is the mass density, and γ is the ratio of specific heats. The subscripts ∞ and 1 are to denote the upstream and downstream regimes, respectively. Equation (3) can then be substituted into Equation (2) in order to relate the solar wind inflow Mach number to the standoff distance.

It should be noted that the empirical relationship in Equation (2) was based on measurements taken for Mach numbers within the range of $5 \leqslant M \leqslant 100$. This relationship also states the shock location approaches a fixed distance away from the obstacle as the Mach number approaches unity, which

Table 1
Spacecraft Positioned at Varying Heliocentric Distances Used in This Study

Spacecraft	Magnetometer	Solar Wind Plasma Analyzer	Data Used for Aspect Ratio Estimates	
			Year	*Rc*
Helios 1	Musmann et al. (1985)	Rosenbauer et al. (1981)	1976–1981	0.3–1 AU
Helios 2	Musmann et al. (1985)	Rosenbauer et al. (1981)	1976–1980	0.3–1 AU
PVO	Russell et al. (1980)	Intriligator et al. (1980)	1978–1988	0.72 AU
Ulysses	Balogh et al. (1992)	Bame et al. (1992)	1991–2004	1.3–5.4 AU
ACE	Smith et al. (1998)	McComas et al. (1998)	1998–2002	1 AU

presents a problem for low Mach numbers. To correct for this, Farris & Russell (1994) hypothesized a new relationship for Equation (3) on the grounds that the shock location should move to infinity as the Mach number approaches unity:

$$\frac{\rho_\infty}{\rho_1} = \frac{(\gamma - 1)M_\infty^2 + 2}{(\gamma + 1)\left(M_\infty^2 - 1\right)}. \quad (4)$$

This relationship yields the same value as Equation (3) for high upstream Mach numbers. If magnetic fields are included in the analysis, Equations (3) and (4) may be converted from the hydrodynamic to the MHD regime. In this case, the effect of the magnetic fields would be to increase the ratio ρ_∞/ρ_1 to above the hydrodynamic value of Equation (3) (Priest & Forbes 2000).

Russell & Mulligan (2002) noted that the empirical constant of 1.1 determined experimentally in Equation (2) was based on an obstacle that had a ratio between the terminator distance (D_T) to the nose distance (D_{OB}) such that, $D_T/D_{OB} = 1.35$. Therefore, for $\gamma = 5/3$, Russell and Mulligan postulated that they could relate the shock standoff distance, Δ, to the radius of curvature, R_c, by combining Equations (2) and (3) to give

$$\frac{\Delta}{R_c} = 0.204 + 0.611M_\infty^{-2}. \quad (5)$$

The terms R_c, D_T, and half the vertical size of a CME ($\frac{1}{2}H$) have been used separately while investigating separate topics, but here we bring these research areas together and define them as the same parameter. While adopting the low Mach number approximation of Farris & Russell (1994) from Equation (4), we obtain

$$\frac{\Delta}{R_c} = 0.204 + \frac{0.815}{\left(M_\infty^2 - 1\right)}. \quad (6)$$

However, Russell & Mulligan (2002) then decided to use a coefficient of 0.78 in Equation (2) instead. This modified relation is a numerical result obtained as a consequence of a spherical obstacle (Seiff 1962) and not the more realistic magnetopause shape by Spreiter et al. (1966). This coefficient then modifies Equations (5) and (6) to

$$\frac{\Delta}{R_c} = 0.195 + 0.585M_\infty^{-2}. \quad (7)$$

$$\frac{\Delta}{R_c} = 0.195 + \frac{0.78}{\left(M_\infty^2 - 1\right)}. \quad (8)$$

The case study example investigated by Russell & Mulligan (2002) was based on in situ data from the *Pioneer Venus Orbiter* (*PVO*) during its approach toward Venus in 1978 August. They obtained the results for R_c (i.e., $\frac{1}{2}H$) from averaging Equations (7) and (8), thereby yielding the conclusion that the aspect ratio of the investigated ICME was approximately 4. It is worth noting here that if Equations (5) and (6) (the more realistic magnetopause morphology) were used instead, the radius of curvature and the aspect ratio would both be reduced to 95.7% of the estimate. Also, if we implemented the MHD version of Equation (3) then the vertical size of the CME would be reduced; therefore, the incorporation of the MHD equation would again reduce our estimate of the aspect ratio.

3. OBSERVATIONS

The coordinate system utilized throughout this study is the radial–tangential–normal (RTN) system which is spacecraft centered, with the radial vector, *R*, directed from the Sun to the spacecraft. The *T*-axis is parallel to the solar equatorial plane and points to the planet motion direction; and the *N*-axis then completes the right-handed triad.

In order to generate estimates of the aspect ratios for ICMEs, our primary goal is to investigate idealized cases that were found at varying heliocentric distances. Here we define idealized cases as clear shock front signatures and magnetic flux rope signatures. For this reason, a thorough investigation of all ICME found within published surveys was not sought due to possible repetition of similar heliocentric distances. The crafts and date ranges presented here may be found in Table 1.

Due to our interest in the CME aspect ratio variation with distance, the *Ulysses* data were selected during 1991–2004. This period includes the spacecraft transit period to Jupiter and the first two full orbital periods. As the *ACE* and *PVO* spacecraft only detects ICMEs at a single heliocentric distance, the full data set available was not inspected. For consistency of analysis all spacecraft magnetic field data were averaged to 10 minute time resolution. Due to the differing plasma instrument capabilities on each spacecraft, the plasma measurements were examined at the highest resolution available in order to calculate the inflow Mach number explained later in Section 4.2. This time resolution varied between 64 s (*ACE*) and 10 minutes (*PVO*). For *Helios* and *PVO*, the solar wind speed magnitude was measured, and therefore assumed to be fully radial when used in later analysis.

In our study, the ICMEs were first identified by using published data sets from ICME surveys for the *Helios* mission (Bothmer & Schwenn 1998), *PVO* (Jian et al. 2008), *Ulysses* (Rees & Forsyth 2003), and *ACE* (Owens & Cargill 2004); however, more complete surveys of ICMEs have been carried out, e.g., by Cane & Richardson (2003); Liu et al. (2005), or Jian et al. (2006). Although these sets of data were used as a starting point, all ICMEs were primarily identified by eye from a combination of a smooth rotation in the magnetic field, enhanced magnetic field magnitude, and a low proton temperature; as can be observed in Figure 2. These three criteria also satisfy the requirements of a subset of ICMEs called magnetic clouds (MCs). However, no single characteristic is taken to be a

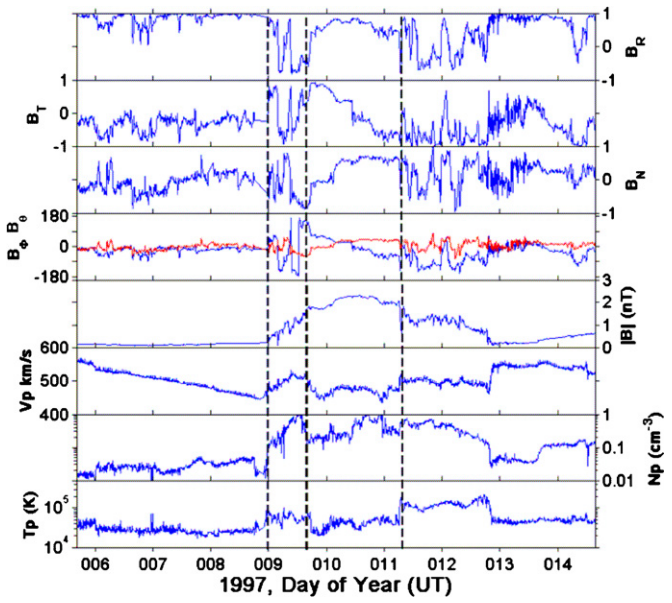

Figure 2. Example event from *Ulysses* in 1997 January at a distance of 1018*Rs*. The vertical dashed lines, from left to right, indicate the position of the shock front, the start point and the end point of the ICME. The magnetic field in RTN coordinates is normalized to the magnitude. Also displayed in the bottom three panels are the proton velocity, proton number density, and the proton temperature. This is an example of an ideal event where the shock normal was obtained by the PMS technique.

(A color version of this figure is available in the online journal.)

necessary condition when other features of magnetic field and plasma are prominent. This explains why we have identified some ICMEs without a clear flux rope signature. For some ambiguous events, where the start and end times were uncertain, a reliable measurement for the ICME radial width was unable to be made and therefore removed from the study.

4. ASPECT RATIO CONSTRUCTION

By approximating the spacecraft to be stationary relative to the propagation of the ICME, in situ measurements directed radially away from the Sun are taken. These measurements are often used to determine the size of a CME by calculating the radial width as the average velocity multiplied by time the CME took to transit over the spacecraft (e.g., Bothmer & Schwenn 1998). This method is a simplification as it does not take into account the orientation and distance of closest approach to the CME center. Also, the CME properties are assumed to remain static for the duration of the CME passing over the spacecraft; this typically takes ∼24 hr at terrestrial distances, whereas in reality, frequent observational evidence has shown that CMEs often expand on this timescale (e.g., Lepping et al. 2008).

4.1. Determining the Shock Normal

The sheath region bounded by the shock front and the ICME leading edge comprises compressed (high-density) plasma and magnetic fields which are often deflected out of the ecliptic plane in order to drape around the ICME (McComas et al. 1989). The draping field lines ahead of an ICME into a plane of compression may lead to the formation of a "planar magnetic structure" (PMS). Nakagawa et al. (1989) first identified them, and suggested various mechanisms for their formation. In these regions, the field lines, although variable, lie in a common plane. Jones et al. (2002) argued that these structures should be present in ICME sheaths with the normal to the plane providing the orientation of the ICMEs' local edge.

By calculating the minimum variance analysis (MVA) direction of the magnetic field in the sheath region ahead of an ICME, we can estimate the direction which corresponds to the normal to the shock plane. We assume the PMS normal is the same as the ICME surface normal, which is then assumed to be the same as the shock normal. The ICME and the shock normal would be parallel if the spacecraft encounter is at the "nose," which we are already assuming with the formulism from Equation (2).

This is our primary method of choice for analysis of ICMEs. An advantage of this analysis over other methods (discussed below) is that the draping of the field lines into a plane of compression occurs on a larger scale, while the others are often used for detailed analysis of the local shock properties. The PMS analysis method should thus provide a more global estimate of the shock normal, as opposed to a more local one estimated by MVA over the shock transition. A single observation made from one entry point into a shock opens up the prospect that the deduced normal may be affected by local variability or waves on the shock surface (Schwartz 2006).

For events exhibiting PMS the shock normal was ultimately determined by applying MVA over the whole sheath region. This is the same method employed by Jones et al. (2002). The result of MVA can be checked by inspecting the eigenvalue ratios between the minimum (λ_3) and the intermediate (λ_2) direction. Hodograms were used as a visual tool and the quantitative ratio was measured; these diagrams track the magnetic field vector projected onto the plane perpendicular to the MVA normal. A consistent requirement of $\lambda_2/\lambda_3 \geqslant 5$ was set throughout the analysis.

Unfortunately, planar structures are not always observed in ICME sheaths, further limiting the number of events suitable for this study. Kataoka et al. (2005) found that PMS structures are best observed for Alfvén Mach numbers above 2; while Jones et al. (2002) found that planar structuring is less likely to form behind a quasi-parallel shock. So for this reason, a second method for determining the shock normal is also implemented—MVA over the shock transition. In this study, this method is predominately used as a verification of the normal vector obtained using the PMS technique.

The orientation of the shock normals was calculated wherever possible by identifying PMS over the sheath region. As a first approximation, similar in process to Jones et al. (2002) and Kataoka et al. (2005), the sheath material applicable for PMS was defined as the interval between the shock and the period where the ICME began. The analysis period was then adjusted visually until the sample fields' ordering remained planar. Generally, the most consistent results were found by taking the full period between the shock and the start of the ICME.

The magnetic field vectors within the measured sheath region were also plotted alongside the plane perpendicular to the PMS normal. Figure 3 displays the results from an event in 1997 January detected by *Ulysses* and shown in Figure 2. The field vectors should follow the curve traced out by the perpendicular plane if PMS is present. The figure shows the normal direction by a "⊕" symbol and the plane perpendicular to the normal shown as a red curve. The scattered points show the direction of the observed magnetic field vectors. These cluster around the plane when PMS is present, whereas for the case where PMS was not observed the vectors can be seen to orientate independently of the plane.

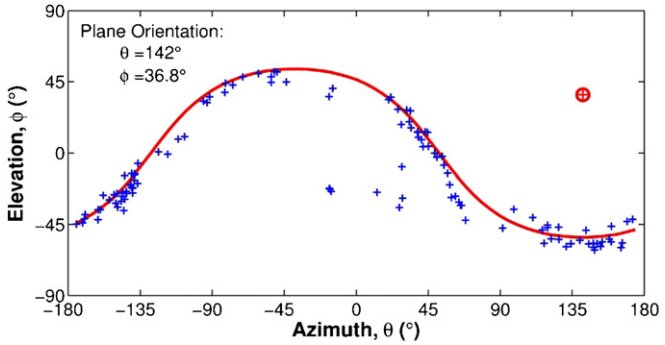

Figure 3. Shock normal displayed by "⊕", and the plane perpendicular to the normal shown as the red curve. Blue scatter points are the individual magnetic field vectors in the sheath region of the 1997 January *Ulysses* event shown in Figure 2.

(A color version of this figure is available in the online journal.)

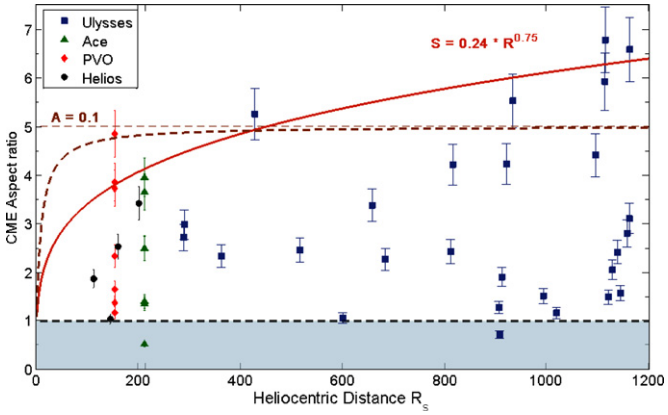

Figure 4. Scatter plot of aspect ratio against heliocentric distance for 45 ICMEs. Brown dashed curve: the geometrical prediction of the ICME aspect ratio for a constant expansion rate ($A = 0.1$); refer to Paper I for more details. Red solid curve: the geometrical prediction by using a varying expansion rate similar to that estimated by Bothmer & Schwenn (1998). The shaded region below a ratio of 1 indicates an oblate CME that would possess a wider radial width than vertical size.

(A color version of this figure is available in the online journal.)

As the shock normal was determined using an MVA procedure, the magnetic field vectors were maintained at an average of 10 minute time resolution throughout the analysis. This averaging of the magnetic field data is often used for magnetic cloud fittings (Lepping et al. 2006). Although this investigation does not discriminate between ICMEs that do and do not observe a signature of flux ropes, it is intriguing to question if this distinction has any relevance to our study.

4.2. CME Selection Process

In situ measurements of ICMEs were inspected by single spacecraft observations identified with four spacecraft. Due to the importance of a shock wave being associated with an ICME in our analysis, only events with a clear shock front present could be used. But as these shock waves only form for fast ICMEs, our analysis effectively investigates a subset of all ICMEs.

We began with a set of 81 candidate events obtained at a range of heliospheric distances and, in the case of *Ulysses*, over varying latitudes. Those with data gaps at crucial times such as at the shock transition for the plasma data or ICME start and end times for the magnetic field were removed from further analysis. Also those events where the uncertainty of the radial width appeared by eye to be more than 20% (i.e., the uncertainty is the start and end times of the ICME) were also discarded; this was determined by the magnetic field, temperature, and number density profile of the ICME.

Events where determination of the shock normal orientation produced uncertain results were also removed. In this study, we accepted the estimated shock orientation if the $\Delta\theta_{\mathrm{Bnu}}$ determined between both methods was less than 15° and the eigenvalue ratios were greater than 5 (Bothmer & Schwenn 1998). But for the events where the $\Delta\theta_{\mathrm{Bnu}}$ for both methods were greater than 15° the events were discarded as unreliable. MVA over the shock transition was used as the sole method to determine the shock normal for seven events, in which the CME possessed a clear flux rope structure with identifiable boundaries but with no clear planar structuring. These results remained in the selection in order to compare the methods of determining the shock normals. The final selection totalled 45 events that are cataloged in the Appendix.

In order to determine the inflow Mach number of the solar wind estimates, the shock speed is required. There are many techniques that use observational data to calculate the shock speed (see Schwartz 1998 for more details on these various techniques). The one chosen for this report uses the mass flux algorithm, which begins with considering the conservation of mass flux across the shock. This method benefits from the ease of application but is limited by its reliance on good plasma density measurements on both sides of the shock (Schwartz 1998).

In this study, the sound speed Mach number is used during the analysis of the ICME aspect ratio. However, estimates of the Alfvén Mach number M_{A} were also generated as a proxy when considering the characteristics of the fast-mode shock preceding the ICME. The fast and slow modes are compressible and more complicated due to their non-isotropic nature. For this reason, the incompressible Alfvén Mach number is often used to characterize a shock (e.g., Kataoka et al. 2005).

5. RESULTS

Once the shock normal was calculated, the upstream Mach number was determined using the procedures described in Section 4.2. The time intervals of the ICME, the Mach number, estimated ratio and comments on individual events are fully listed as a table in the Appendix. Aspect ratio is plotted against heliocentric distance in Figure 4. Each event is individually represented by the scatter plot which displays the events by spacecraft. The results are plotted alongside theoretical predictions made from assuming a kinematic propagation of a flux-rope-like structure (see Paper I for more details).

The results from the 45 events show that they are predominately elliptical. The mean and standard deviation of the aspect ratio from our sample are 2.8 and 1.55, respectively. By assuming our sample is normally distributed, the 95% confidence interval for our aspect ratio estimate is 2.8 ± 0.5. This strongly supports that fast ICMEs are elliptical, and have significantly evolved away from the circular cross section found in the high solar corona and estimated by remote observations from the HI instrument on board *STEREO* (Savani et al. 2009). Figure 5 displays a histogram of the aspect ratio; this figure also displays a Gaussian distribution using the mean and standard deviation calculated earlier. Other than the aspect ratio being a continuous variable, our results appear to better fit a Poisson distribution. This could be due to a possible extended tail which may result from an expansion velocity that varies with distance. This implies the aspect ratio is likely to increase with distance;

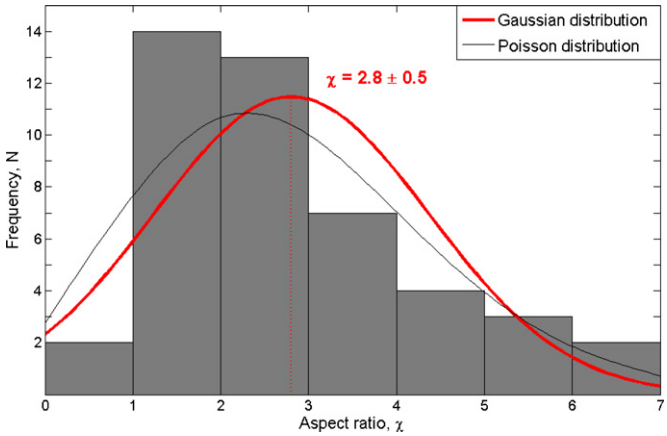

Figure 5. Histogram of the aspect ratios of 45 ICME events from Figure 4. Shown in red is the Gaussian distribution with the same mean (2.8) and standard deviation (1.55) as the observations. The black curve is the estimated Poisson distribution. Labeled in red is the estimated average aspect ratio with a confidence interval of 95%.

(A color version of this figure is available in the online journal.)

therefore, a "tail" of large aspect ratios is likely to form if more events at larger distances are introduced.

5.1. Uncertainty in Aspect Ratio Values

As Equations (7) and (8) predict the aspect ratio would be highly dependent on the Mach number, which itself requires the shock normal, the uncertainty of determining this vector provides the single biggest uncertainty in our results. To study the uncertainty in the normal, five example events were taken, four using the PMS analysis and one using the MVA. For these examples the normal was rotated in the azimuthal and meridional direction in 2° increments for a maximum deviation of 15° for each direction. For each new vector the aspect ratio was recalculated. This provides a geodesic square on a surface of a sphere within which the aspect ratio was determined. Figure 6 shows the resulting surface for our 1997 *Ulysses* case study event. For display purposes, a larger maximum deviation of 30° is shown. The color map displays the aspect ratio changing with shock normal direction, such that a local maximum value is often located in close proximity to the best estimate for the shock normal. For each of the five events the average and standard deviation of the aspect ratio were determined. These results showed a standard deviation of the order of 6% of the calculated ratio.

As is often the case, there are other sources of uncertainty inherent within this analysis, such as the justification of the empirical formula that underpins the inferred vertical size of a CME; this is likely to cause a systematic error and therefore perhaps shift the results to be centered on the geometrical predictions. The other significant uncertainty is the identification of the start and end timings of each ICME. This is significant albeit somewhat difficult to quantify (Lepping et al. 2003). For this reason, it was felt reasonable to increase the total uncertainty in our aspect ratio to an approximate, but realistic, 10%. This uncertainty margin is plotted as error bars on Figure 4.

5.2. Correlating Aspect Ratio with Other Parameters

We did not distinguish between high- and low-latitude CMEs in our study, even though Gosling et al. (1998) had noticed that many ICMEs which are ejected from high latitudes behave differently to the low-latitude ICMEs—they sometimes exhibit

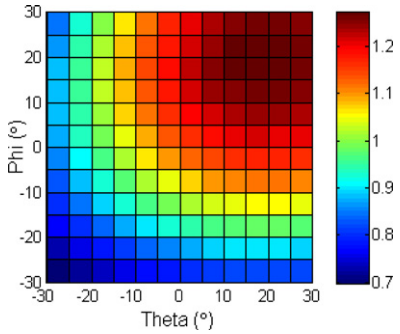

Figure 6. Surface map for the varying aspect ratio with possible shock normal direction. The figure is centered on the best estimate of the shock normal from PMS analysis. The surface displays a geodesic square on a sphere, centered on the estimated shock normal direction. This is an example from the 1997 *Ulysses* event displayed in Figure 2; displaying an aspect ratio of 1.2.

(A color version of this figure is available in the online journal.)

a forward and reverse shock. The authors suggested this was due to high internal pressures and termed these ICMEs to be overexpanding. We note that within our selection six *Ulysses* events were observed at latitudes of greater than 40°. The aspect ratio of these ICMEs varied between 1.1 and 5.3 while their upstream Mach numbers ranged between 1.2 and 4.4. There appears to be no correlation between latitude and either Mach number or the resulting aspect ratios, although a full statistical analysis cannot be carried out due to the low number of events.

Figure 7 displays the Mach number of the same 45 CME events as in Figure 4. Here, we are not able to observe any correlation between the Mach number of an individual event and its aspect ratio or its heliocentric distance. Similarly, no correlation was observed with the Alfvén Mach number. For completeness we also investigated the possibility that the angle between the upstream magnetic field and the shock normal (defined as the θ_{Bn}) may also have a correlation to our aspect ratio and heliocentric distance. But we do not find any significant evidence for a correlation. Figure 8 displays the color-coded results according to the θ_{Bn}; our analysis is not concerned with whether the magnetic field is pointing into or out of the shock and therefore θ_{Bn} varies from 0° to 90°. If we consider the θ_{Bn} values in two categories of less than and greater than 1 AU, we find the averages are 52° ± 19° (18 events) and 70° ± 20° (27 events), respectively. These results do indicate a slight preference for a quasi-perpendicular shock further out into the heliosphere. This is perhaps to be expected if the shock normal of the CME is considered to preferentially point radially away from the Sun and the magnetic field is on average following the parker spiral.

Further investigation into the individual CME parameters against the aspect ratio is beyond the scope of this paper, but further work may consider analyzing CME bulk flow, total magnetic field strength, or chirality against the aspect ratio over varying heliocentric distance. However, as the shock itself can be characterized by MHD parameters, it is worth noting that if the Alfvén Mach number is implemented in the analysis of the aspect ratio, the results would have been similar. The mean aspect ratio under these conditions would yield a value of 2.6 ± 0.4.

6. DISCUSSION

Our study shows that there is strong evidence for the cross section of ICMEs to be elliptical and not circular. This idea alone

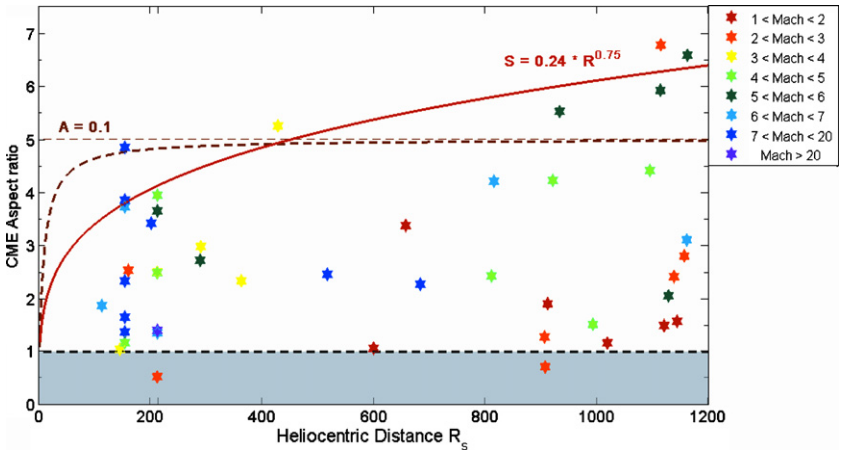

Figure 7. Same as Figure 4, but the individual color-coded events are defined by the calculated inflow sound speed Mach number.
(A color version of this figure is available in the online journal.)

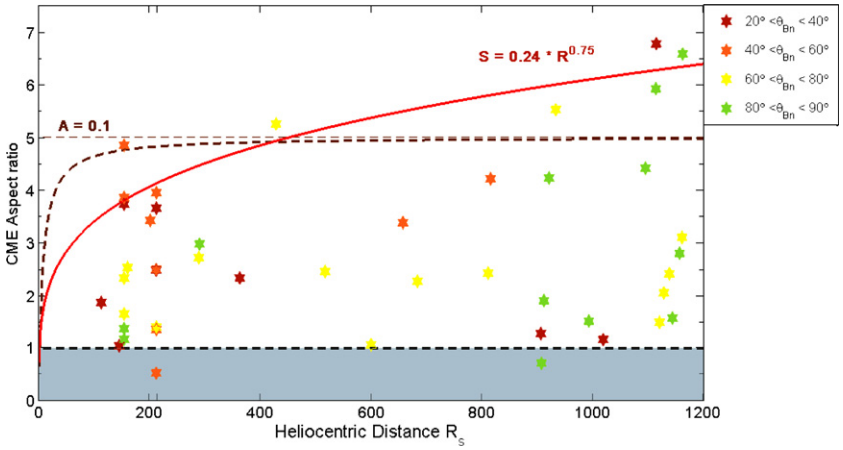

Figure 8. Same as Figure 4, but the individual color-coded events are defined by the calculated $\theta_{\rm Bn}$.
(A color version of this figure is available in the online journal.)

is not new and has been investigated previously using various methods (e.g., Riley & Crooker 2004; Odstrcil et al. 2005; Owens et al. 2006). Previously, work has been undertaken both observationally (e.g., Russell & Mulligan 2002; Liu et al. 2006) and through simulations to quantify the aspect ratio of ICMEs in the heliosphere. However, unlike previous observational studies which have been focused on case studies at a fixed heliocentric distance, the work presented here is the first attempt to statistically quantify the cross-sectional elongation of ICMEs and to monitor its evolution with heliocentric distance. We compare this to simple geometrical predictions of an aspect ratio which estimates a value between 3 and 6, and that if a constant rate of expansion is assumed (Russell & Shinde 2003; Forsyth et al. 2006) the geometry predicts the aspect ratio to converge to a fixed value and become scale invariant as indicated by Savani et al. (2010).

However, many assumptions have been included in this analysis and the aspect ratio from all the events presented here is scattered with a large standard deviation with respect to the mean. They also do not follow the predicted geometrical model. For these reasons, it is prudent to bring a critical eye to the conclusions and identify the assumptions and limitations to this study.

First, a significant proportion of ICMEs were found to have aspect ratios between ∼1 and 2. Also, if the MHD relationship for the density ratio in Equation (3) was used, then an even larger fraction of our CMEs would fall within this category. This suggests that a large fraction of events appear to be quasi-circular in cross section. If the results suggesting a circular cross section are to be believed then the question to ask is, how can this be true while the CME still propagates radially away from the Sun? One possible solution is to appreciate that a CME should not be treated as a solid object travelling through a plasma, but an object that may interact and be distorted by its surroundings (Kahler & Webb 2007). Using the inner HI camera on *STEREO-A*, Savani et al. (2010) monitored the distorting of a CME's leading edge into a concave shape. This leading edge distortion reduces the radius of curvature of the CME; at least locally around the position of the transiting spacecraft. As our method of analysis is in fact measuring the radius of curvature, then this may be evidence for a significant proportion of all CMEs to possess a distorted leading edge. As this analysis also limits the study to fast CMEs with associated shock fronts, then this suggests the structure of CMEs is often distorted by propagating into slower streams of solar wind ahead; thereby creating perhaps a wave-like shape for the leading edge. Previous studies using in situ

data have attempted to provide evidence of global distortions with mixed results (Liu et al. 2006, 2008; Owens 2006). But to an extreme, Owens (2009) conceptually hypothesized magnetic reconnection from the presence of a current sheet within an elongated ICME may create multiple mini-CMEs. The work presented by Savani et al. (2010) suggests a similar outcome but driven by the interaction between the ICME and the solar wind—creating a distortion to the ICME morphology. This would then lead to the appearance of ICMEs with more circular cross sections when measured in situ.

Another important concern is the evolving nature of ICMEs. Owens et al. (2006) showed that a radial cut through a model at a fixed point in time can give a significantly different result to a model that evolves a magnetic flux rope in time past a fixed position. This is simply because the morphology of the ICME changes in the time taken to pass over the spacecraft. This is important as we are assuming an inferred vertical size of a CME at the beginning of the transit, but only measure the full width of the CME at the time when the spacecraft exits the transit. Therefore, this implies our method would generate a more circular structure than the reality.

Our estimation of the vertical size of the CME is based on determining the radius of curvature of the ICME front edge. This radius of curvature physically depends on both the curved axis of the rope structure and the vertical size of the ICME in the direction perpendicular to the radial and the rope axis. Our procedure also assumes the spacecraft always passes through the ICME center, with the empirical relationship being derived from studies about the radius of curvature on a magnetosphere at the nose. This is a simplification to the problem. If a new empirical relationship could be generated for impacts that occurred away from the nose of a magnetosphere then improvements to this study may be attempted. By optimizing a constant-alpha force-free flux rope model to the in situ data, the impact parameter may be determined. This distance of closest approach can then be used with the new empirical relationship, and perhaps the aspect ratios may provide more realistic comparisons to the geometrical model.

The shapes of ICMEs and magnetospheres are different on global scales; magnetospheres may be regarded as isolated objects that are more or less spherical; whereas ICMEs are often considered to be more cylindrical with "legs" that curve back to the Sun. Siscoe & Odstrcil (2008) used simulations to investigate the properties of the sheath region between ICMEs and their associated shock front. They propose that due to the expansion of ICMEs, the ICME sheath region may qualitatively differ from planetary sheaths. These authors simulated the solar wind interaction with Earth's magnetosphere and a fast ICME. The spatial scales were normalized in order to make a direct comparison. They argued that solar wind piles up in front of an ICME instead of flowing around it, and resulting in ICME sheaths thinner than those of planetary magnetosheaths. This suggests our correlation of planetary shocks and ICME shocks may be misplaced, but their conclusions are yet to be supported observationally. A thinner sheath region would suggest our results may be lower estimates, and all the calculated CME aspect ratios should be systematically larger. A possible correction for this would be to deduce a new empirical formula, based on the equation by Spreiter et al. (1966). That is to say, the factor of 1.1 as a constant of proportionality in Equation (2) and $D_T/D_{OB} = 1.35$ should be different for ICMEs.

Previous ICME surveys have highlighted the large event-to-event variability in their internal structure and with the solar wind (e.g., Bothmer & Schwenn 1994, 1998), and this was also to be expected for our study. However the new HI camera on the *STEREO* mission has a larger field of view than previous coronagraph instruments (Eyles et al. 2009). This enables remote observations at distances further away from the Sun, where only in situ measurements had been previously available (e.g., Davis et al. 2009; Liu et al. 2010a, 2010b; Mostl et al. 2009; Rouillard et al. 2009, 2010a, 2010b, 2010c). Therefore, similar to the work by Savani et al. (2009, 2010), the evolving aspect ratio of a single ICME may be investigated over large distances. In the future, it is hoped that these types of detailed studies may substantially reduce this variability caused between events.

7. CONCLUSIONS

A survey of 45 ICMEs, from four spacecraft at different heliocentric distances, was carried out. These results provide an average aspect ratio of 2.8 ± 0.5, clearly indicating that ICMEs have deviated away from the ideal cylindrical structure with a circular cross section. These results show that the measured aspect ratios are consistently below the predicted geometrical estimates but above one. Therefore, these results display evidence that distortion away from a self-similar expansion of a cylindrical flux rope exists, such that the ICME becomes elliptical as it propagates away from the Sun, but not to the extent that would have been predicted if the ICME propagated radially away from the Sun. The results also show that if a CME can be observed remotely by coronagraphs and its angular width can be determined, then with high probability ($\sim$90%), an upper bound aspect ratio can be determined for this CME anywhere between the Sun and 5.5 AU, simply by making an estimate for a constant rate of expansion.

If Equation (3) is converted to the MHD relation and the empirical relationship of standoff distances for bow shocks is to be trusted for ICME shocks, as suggested by Russell & Mulligan (2002), then the circular results may indicate distortions to the structure of the CMEs leading edge, i.e., reducing the radius of curvature (Savani et al. 2010). Our results suggest this would then be a frequent occurrence.

On the other hand, if the empirical formula is needed to change as suggested by Siscoe & Odstrcil (2008), then values in out aspect ratios should be increased to a more elliptical object. A new constant for the empirical relation would need to be devised for shocks associated with ICMEs.

N.P.S. thanks E. M. Henley, J. Mitchell, T. S. Horbury, and S. J. Schwartz of Imperial College London. We are grateful for the magnetic field data from *PVO* (PI: C. T. Russell), *Helios* (PI: F. B. Neubauer), *Ulysses* (PI: A. Balogh), and *ACE* (PI: N. Ness), and the solar wind plasma data from *PVO* (PI: A. Barnes), *Helios* (PI: H. Rosenbauer), *Ulysses* (PI: D. J. McComas), and *ACE* (PI: G. Gloeckler). N.P.S also thanks the Japan Society for the Promotion of Science (JSPS) for the support and award of a fellowship. This work was also partly supported by UK STFC through the award of a PhD studentship at Imperial College London.

APPENDIX

The time intervals of the ICME, the Mach number, estimated ratio, and comments on individual events are fully listed in Table A1.

Table A1
A Selected CME Survey over Multiple Spacecraft through Solar Cycle 21- 23, for Their Shock Fronts and PMS Configuration in the Sheath

Spacecraft	Year	DOY	Shock	CME		Distance,	Mach #	θ_{Bn}	Aspect	Shock	Comments
				Start Time	End Time	*Rs*			Ratio		
Helios 1	1977	335	05.02	13.37	23.05	161.3	2.1	62.2	2.5	MVA	PMS and MVA similar results. MVA used as better ratio.
Helios 2	1978	003	14.32	7.55+24	17.48+48	202.2	14.9	56.2	3.4	PMS	Some data gaps in mag. Data in sheath region—plasma seems ok. PMS Eigen ratio much better than MVA.
Helios 2	1979	092	19.32	04.11+24	13.28+48	146.3	3.0	20.1	1.0	PMS	Clear data FR. Both normal methods very consistent.
Helios 1	1980	171	19.06	1.55+24	19.46	114.0	6.9	24.1	1.9	PMS	PMS good. But limited selection taken. Eigen ratio better than MVA.
PVO	1979	007	22.22	9.47+24	22.31+24	154.9	6.1	34.5	3.7	MVA	PMS bad. CME is clear but not quite ideal. MVA good, eigen ratio
PVO	1979	202	15.07	20.14	08.11+24	154.9	11.0	82.3	1.4	PMS	PMS good, but with very few data points. Linear vel profile. But not clean Flux rope structure
PVO	1980	098	0.32+24	11.22	05.21+48	154.9	9.3	69.7	2.3	PMS	PMS good—but only if use early section.
PVO	1981	201	12.36	19.35	10.19+24	154.9	14.8	79.0	1.7	MVA	PMS bad. NOT great example. Velocity data gap.
PVO	1983	129	10.33	22.37	11.14+24	154.9	19.1	49.2	4.8	PMS	PMS ok when using select interval. PMS consistent with MVA but with great eigen ratio.
PVO	1984	039	12.01	04.44+24	06.49+48	154.9	9.5	47.5	3.9	PMS	PMS good. CME clear FR
PVO	1984	048	09.21	14.08	2.28	154.9	4.7	83.7	1.2	PMS	PMS ok. CME nice. FR shock ok. Data gaps in relevant places made calculation not completely accurate.
ACE	1998	063	08.59	15.08	20.01+24	213.0	2.6	55.0	0.5	MVA	PMS very bad. Few data points. MVA used. Correlates to perpendicular to axis from FR model.
ACE	1998	267	21.14	06.48+24	15.44+48	213.0	41.7	61.9	1.4	PMS	Great PMS. Eigen ratio only maginaly better than MVA. Large Mach #.
ACE	1999	106	09.59	22.12	18.41+24	213.0	3.4	46.8	2.5	PMS	Good FR mag. field. But PMS is ok if use mid section only.
ACE	2000	311	08.01	22.06	16.04+24	213.0	5.3	39.2	3.7	PMS	PMS good if use mid section only. FR Clear Bfield rotation.
ACE	2001	101	11.32	08.01+24	06.56+48	213.0	4.9	51.4	3.9	MVA	PMS is very bad. Clear mag field FR.
ACE	2001	304	12.06	20.50.	05.51+48	213.0	6.1	47.9	1.4	PMS	PMS ok/good. Clear Bfield rotation.
ACE	2002	230	16.16	18.19+24	20.14+72	213.0	4.6	32.4	2.5	MVA	PMS bad. Mag. field FR not obvious.
Ulysses	1991	074	05.11	05.50+24	12.55+72	517.2	7.3	79.5	2.5	PMS	MVA good. Good eigen ratio.
Ulysses	1991	147	03.24	09.24+48	16.30+168	683.7	8.8	78.5	2.3	PMS	MVA good. Eigen ratio ok/good
Ulysses	1991	261	05.42	13.12	10.59+24	907.0	2.1	87.2	0.7	PMS	MVA good. Eigen ratio good. Very small FR. possible interaction with fast wind from behind—i.e. reconnection and loss of magnetic flux leading to a reduction in aspect ratio
Ulysses	1992	052	08.01	9.43+72	19.18+120	1161.4	6.0	89.7	6.6	PMS	PMS ok. Eigen ratio not great.
Ulysses	1992	307	04.38	01.19+24	17.26	1113.0	5.4	85.4	5.9	PMS	MVA good. Non ideal velocity profile. Strong velocity jump just ahead of interaction region.

Table A1
(Continued)

Spacecraft	Year	DOY	Shock	CME		Distance,	Mach #	θ_{Bn}	Aspect	Shock	Comments
				Start Time	End Time	*Rs*			Ratio		
Ulysses	1997	008	23.24	17.22+24	04.29+72	1018.4	1.7	23.6	1.2	PMS	PMS very good. Solar wind profile not ideal but good.
Ulysses	1997	216	17.13	15.10+24	15.37+48	1119.7	1.4	74.4	1.5	PMS	PMS very good. Nearly perfect.
Ulysses	1997	241	07.54	03.07+24	09.34+48	1127.7	5.6	71.2	2.1	PMS	PMS ok. Not large CME or sheath. But distinct velocity jump.
Ulysses	1997	275	05.33	15.19+24	07.02+72	1137.4	2.4	72.7	2.4	PMS	PMS very good. Good velocity jump. But not perfect velocity profile inside FR.
Ulysses	1997	298	19.49	01.03+72	07.34+120	1143.1	1.3	82.8	1.6	PMS	PMS very good.
Ulysses	1999	012	20.35	15.33+48	10.12+72	1113.7	2.3	27.1	6.8	PMS	PMS ok. But used only because MVA was consistent.
Ulysses	1999	060	00.03+24	21.24+48	22.12+96	1094.6	4.8	88.8	4.4	PMS	PMS ok if using a select range. FR start difficult to define. MVA bad.
Ulysses	1999	344	00.08+24	07.07+72	04.44+120	911.3	1.2	86.5	1.9	PMS	PMS ok. FR not ideal. Eigen ratio not good. MVA bad. Latitude $> 40^\circ$.
Ulysses	2000	090	00.10+24	12.21	08.22+48	810.9	4.4	74.2	2.4	PMS	PMS is very good. CME is clear FR. Ideal case but small/medium sized. Latitude $>40^\circ$.
Ulysses	2001	004	22.45	20.11+24	13.11+48	428.8	3.8	68.7	5.3	PMS	PMS ok. Suspect there is a double FR occuring but only first half used in analysis. Latitude $>40^\circ$.
Ulysses	2001	156	01.30	19.49	19.06+24	289.7	5.0	68.2	2.7	PMS	PMS looks promising—dubious when defining CME trailing edge. Appearance of current sheet within CME.
Ulysses	2001	159	23.28	05.34+48	19.54+72	291.1	3.1	87.0	3.0	PMS	PMS ok. Large difference between q_{Bn} for MVA and PMS—definition of shock front and FR extent is diffiult.
Ulysses	2001	236	07.26	14.41	00.51+24	363.4	3.0	33.5	2.3	PMS	PMS ok but need to be very careful with interval. Large difference with MVA and PMS. Accepted in final selection, but dubious. Latitude $>40^\circ$.
Ulysses	2002	030	21.11	16.06+24	23.45+48	600.0	1.5	78.1	1.1	PMS	PMS good, but MVA with slightly different results. Latitude $>40^\circ$.
Ulysses	2002	073	04.08	22.11	07.43+24	657.6	1.4	42.8	3.4	PMS	PMS ok. MVA eigen ratios not good. Latitude $>40^\circ$.
Ulysses	2002	205	21.17	16.15+24	13.31+48	815.3	6.2	50.6	4.2	PMS	Time profile is excellent, but PMS is ok only if used with very careful interval. MVA is very bad. Trailing edge very difficult to define. Possible double FR so used only selection with rotation.
Ulysses	2002	298	14.38	16.07+24	08.47+96	905.9	2.4	38.0	1.3	PMS	CME is great but PMS is only ok/bad with specific dirn. Looks like overexpanding CME. Larger error in aspect ratio due to shock normal uncertainty.
Ulysses	2002	316	19.54	05.27+24	15.39	920.7	4.6	89.1	4.2	PMS	PMS good. MVA is consistent. But CME is small.
Ulysses	2002	331	05.46	18.41	04.33+24	933.0	5.5	78.4	5.5	PMS	PMS good. MVA not consistent. CME is small.
Ulysses	2003	043	05.27	16.33	00.28+48	992.3	4.0	85.8	1.5	MVA	MVA good. Clear shock. PMS eigen ratio was bad. FR start and end time difficult to define. Possible double FR mixed together. Creates large aspect ratio uncertainty.
Ulysses	2004	234	12.32	18.10+48	03.45+144	1160.3	6.3	63.4	3.1	PMS	MVA ok. Close to ideal case.
Ulysses	2004	280	07.45	03.06+48	08.27+96	1155.8	2.7	88.7	2.8	PMS	MVA ok/good. Complication with compression from fast SW.

REFERENCES

Balogh, A., et al. 1992, A&A, 92, 221
Bame, S. J., et al. 1992, A&A, 92, 237
Bothmer, V., & Schwenn, R. 1994, Space Sci. Rev., 70, 215
Bothmer, V., & Schwenn, R. 1998, Ann. Geophys., 16, 1
Burlaga, L. F. 1988, J. Geophys. Res., 93, 7217
Cane, H. V., & Richardson, I. G. 2003, J. Geophys. Res., 108, 1156
Davis, C. J., Davies, J. A., Lockwood, M., Rouillard, A. P., Eyles, C. J., & Harrison, R. A. 2009, Geophys. Res. Lett., 36, L09108
Eyles, C. J., et al. 2009, Sol. Phys., 254, 387
Farris, M. H., & Russell, C. T. 1994, J. Geophys. Res., 99, 17681
Forsyth, R. J., et al. 2006, Space Sci. Rev., 123, 383
Gosling, J. T., Riley, P., McComas, D. J., & Pizzo, V. J. 1998, J. Geophys. Res., 103, 1941
Hu, Q., & Sonnerup, B. U. O. 2002, J. Geophys. Res., 107, 1142
Intriligator, D. S., Wolfe, J. H., & Mihalov, J. D. 1980, IEEE Trans. Geosci. Remote Sens., 18, 39
Jackson, B. V., Boyer, J. A., Hick, P. P., Buffington, A., Bisi, M. M., & Crider, D. H. 2007, Sol. Phys., 241, 385
Jian, L. K., Russell, C. T., Luhmann, J. G., & Skoug, R. M. 2006, Sol. Phys., 239, 393
Jian, L. K., Russell, C. T., Luhmann, J. G., Skoug, R. M., & Steinberg, J. T. 2008, Sol. Phys., 249, 85
Jones, G. H., Rees, A., Balogh, A., & Forsyth, R. J. 2002, Geophys. Res. Lett., 29, 1520
Kahler, S. W., & Webb, D. F. 2007, J. Geophys. Res., 112, A09103
Kataoka, R., Ebisuzaki, T., Kusano, K., Shiota, D., Inoue, S., Yamamoto, T. T., & Tokumaru, M. 2009, J. Geophys. Res., 114, A10102
Kataoka, R., Watari, S., Shimada, N., Shimazu, H., & Marubashi, K. 2005, Geophys. Res. Lett., 32, L12103
Landau, L. D., & Lifshitz, E. M. 1959, Fluid Mechanics (London: Pergamon),
Lepping, R. P., Berdichevsky, D. B., & Ferguson, T. J. 2003, J. Geophys. Res., 108, 1356
Lepping, R. P., Jones, J. A., & Burlaga, L. F. 1990, J. Geophys. Res., 95, 11957
Lepping, R. P., Wu, C. C., Berdichevsky, D. B., & Ferguson, T. 2008, Ann. Geophys., 26, 1919
Lepping, R. P., et al. 2006, Ann. Geophys., 24, 215
Liu, Y., Davies, J. A., Luhmann, J. G., Vourlidas, A., Bale, S. D., & Lin, R. P. 2010a, ApJ, 710, L82
Liu, Y., Manchester, W. B., Richardson, J. D., Luhmann, J. G., Lin, R. P., & Bale, S. D. 2008, J. Geophys. Res., 113, A00B03
Liu, Y., Richardson, J. D., & Belcher, J. W. 2005, Planet. Space Sci., 53, 3
Liu, Y., Richardson, J. D., Belcher, J. W., Wang, C., Hu, Q., & Kasper, J. C. 2006, J. Geophys. Res., 111, A12S03
Liu, Y., Thernisien, A., Luhmann, J. G., Vourlidas, A., Davies, J. A., Lin, R. P., & Bale, S. D. 2010b, ApJ, 722, 1762
Lugaz, N., Manchester, W. B., & Gombosi, T. I. 2005, ApJ, 627, 1019
Manchester, W. B., et al. 2004, J. Geophys. Res., 109, A01102
Marubashi, K. 1997, in Coronal Mass Ejections, ed. N. U. Crooker, J. A. Joselyn, & J. Feynman (New York: AGU), 147
McComas, D. J., Bame, S. J., Barker, P., Feldman, W. C., Phillips, J. L., Riley, P., & Griffee, J. W. 1998, Space Sci. Rev., 86, 563
McComas, D. J., Gosling, J. T., Bame, S. J., Smith, E. J., & Cane, H. V. 1989, J. Geophys. Res., 94, 1465
Mostl, C., et al. 2009, ApJ, 705, L180
Mulligan, T., & Russell, C. T. 2001, J. Geophys. Res., 106, 10581
Musmann, G., Neubauer, F. M., Maier, A., & Lammers, E. 1985, Raumfahrt-forschung, 19/5, 232
Nakagawa, T., Nishida, A., & Saito, T. 1989, J. Geophys. Res., 94, 11761
Nakamizo, A., Tanaka, T., Kubo, Y., Kamei, S., Shimazu, H., & Shinagawa, H. 2009, J. Geophys. Res., 114, A07109
Odstrcil, D., Pizzo, V. J., & Arge, C. N. 2005, J. Geophys. Res., 110, A02106
Odstrcil, D., Riley, P., & Zhao, X. P. 2004, J. Geophys. Res., 109, A02116
Owens, M. J. 2006, J. Geophys. Res., 111, A12109
Owens, M. J. 2009, Sol. Phys., 260, 207
Owens, M. J., & Cargill, P. 2004, Ann. Geophys., 22, 661
Owens, M. J., Merkin, V. G., & Riley, P. 2006, J. Geophys. Res., 111, A03104
Priest, E. R., & Forbes, T. G. 2000, in Magnetic Reconnection: MHD Theory and Applications, (Cambridge: Cambridge Univ. Press), 1
Rees, A., & Forsyth, R. J. 2003, Geophys. Res. Lett., 30, 8030
Riley, P., & Crooker, N. U. 2004, ApJ, 600, 1035
Riley, P., Linker, J. A., & Mikic, Z. 2001, J. Geophys. Res., 106, 15889
Rosenbauer, H., et al. 1981, in Luft-und Raumfahrt, Weltaumforschung/ Weltraumtechnologie, BMFT-FB, W81–015
Rouillard, A. P., et al. 2009, J. Geophys. Res., 114, A07106
Rouillard, A. P., et al. 2010a, J. Geophys. Res., 115, A04103
Rouillard, A. P., et al. 2010b, J. Geophys. Res., 115, A04104
Rouillard, A. P., et al. 2010c, ApJ, 719, 1385
Russell, C. T., & Mulligan, T. 2002, Planet. Space Sci., 50, 527
Russell, C. T., & Shinde, A. A. 2003, Sol. Phys., 216, 285
Russell, C. T., Snare, R. C., Means, J. D., & Elphic, R. C. 1980, IEEE Trans. Geosci. Remote Sens., 18, 32
Savani, N. P., Owens, M. J., Rouillard, A. P., Forsyth, R. J., & Davies, J. A. 2010, ApJ, 714, L128
Savani, N. P., Rouillard, A. P., Davies, J. A., Owens, M. J., Forsyth, R. J., Davis, C. J., & Harrison, R. A. 2009, Ann. Geophys., 27, 4349
Savani, N. P., Rouillard, A. P., Owens, M. J., Forsyth, R. J., Kusano, K., Shiota, D., & Kataoka, R. 2011, ApJ, 731, 109
Schwartz, S. J. 1998, in Analysis Methods for Multi-spacecraft Data, ed. G. Paschmann & P. W. Daly (Bern: ISSI), 249
Schwartz, S. J. 2006, Space Sci. Rev., 124, 333
Seiff, A. 1962, in Gas Dynamics in Space Exploration, Recent Information on Hypersonic Flow Fields, (NASA SP-24; Washington, DC: NASA), 269
Shiota, D., Kusano, K., Miyoshi, T,., & Shibata, K. 2010, ApJ, 718, 1305
Siscoe, G., & Odstrcil, D. 2008, J. Geophys. Res., 113, A00B07
Smith, C. W., L'Heureux, J., Ness, N. F., Acuna, M. H., Burlaga, L. F., & Scheifele, J. 1998, Space Sci. Rev., 86, 613
Spreiter, J. R., Summers, A. L., & Alksne, A. Y. 1966, Planet. Space Sci., 14, 223
Wang, C., Du, D., & Richardson, J. D. 2005, J. Geophys. Res., 110, A10107